DESIGN AND EXPERIMENTAL STUDIES OF MULTILAYER COATING FOR APPLICATIONS IN GALLIUM NITRIDE LIGHT EMITTING DEVICES

by

NASER MAHMOUD AHMED

Thesis submitted in fulfillment of the requirements for the degree of Doctor of Philosophy

JUNE 2006

ACKNOWLEDGMENTS

I want to give my sincere appreciation to my thesis advisor, Dr. Md. Roslan Hashim, for the discussion on the directions of research for this study, and the consistent encouragement on the experiments. His valuable advice in many other matters is also highly appreciated. I also would like to sincerely thank Dr. Zainuriah Hassan, for additional advice and help. Without her patience, guidance and constant supports, this work would not have been possible.

Thanks also go to the offices of Universiti Sains Malaysia, School of Physics, IPS, Dean, both deputy Deans and all the staff in the main office. The friendship and assistance from the students at NOR laboratory are also appreciated. Finally, I want to give my special thank to my lovely wife, Kifah, for supporting me, sacrificing her time, and understanding the difficulty to pursue and complete this PhD degree and my two lovely sons – Hamza and Shaemaa' for asking me when I could graduate. I want to give my great honor to my parents, my brothers and my sisters for their support and encouragement, especially to my father who never had the chance to see me getting this degree.

TABLE OF CONTENTS

TABLES CAPTIONS

FIGURES CAPTIONS

LIST OF SYMBOLS

Abbreviations

AFM	Atomic Force Microscopy.
Ag	Silver
Al	Aluminum
ATR	Attenuated Total Reflection
CAIBE	Chemical assisted ion beam etching
CCD	Charge-coupled device
CVD	Chemical Vapour Deposition.
CW	Continuous wavelength
DBR	Distributed Bragg reflector
DC	Direct Current.
EM	Electromagnetic
FWHM	Full Width at Half Maximum.
GaAs	Gallium Arsenide
GaN	Gallium Nitride
GaP	Gallium Phosphate
HfO_2	Hafnium oxide
InGaN	Indium Gallium Nitride
LD	Laser diode
LED	Light Emitting Diode.
LEEBI	Low energy electron beam irradiation
MATLAB	Matrix laboratory
MBE	Molecular Beam Epitaxy.
Mg	Magnesium
MOCVD	Metalorganic Chemical Vapour Deposition.
MOVPE	Metal–organic vapour phase epitaxy
N_2	Nitrogen
OMVPE	Organometallic vapor phase epitaxy
PEC	Photo electrochemical etching
PL	Photoluminescence
PVD	Physical Vapour Deposition.
QWOT	Quarter wave optical thickness
RCLEDs	Resonant-cavity light emitting diodes
RIE	Reactive ion etching
RT	Room temperature
SiO_2	Silicon dioxide
SP	Surface plasmons
SPP	Surface plasmon polariton
TE	Transverse electric field
TiO_2	Titaniun dioxide
TIR	Total internal reflection
TM	Transverse magnetic field
TMM	Transfer matrix method
UV	Ultraviolet
VCSEL	Vertical cavity surface emitting lasers
WBGS	Wide bandgap semiconductors

Roman Symbols:

n	Refractive index
N	Number of layers
n_0	Refractive index of the incident medium (usually air)

E	Electric field
H	Magnetic field
n_s	Refractive index of the substrate
t_{ij}^{μ}	Total electric field transmission at interface J
t_{ij}	Amplitude coefficients of transmission
r_{ij}	Amplitude coefficients of reflection
Y	Optical admittance of the assembly
T	Transmittance
R	Reflectivity
r	Reflection coefficient
d	Film thickness.
k_z	Wavevector
$\bar{s}$	Unit vector along the direction of the electric field
$R_{A;s}$	Intensity reflectance at the film–air interface
$\hbar\omega_{BG}$	Bandgap energy
$\hbar\omega_{SP}$	Surface plasmon energy
$R_{B;p}$	Intensity reflectance at the film-substrate interface

Greek Symbols:

η_{sub}	Optical admittance of the substrate
Ψ	Phase changes on reflection
Δn	Index contrast
θ_c	Critical angle
δ_1	Phase retardation in the thin film layer
ω	Circular frequency
λ_0	Wavelength of incident light in a vacuum
η_1	Optical admittance of the thin film layer
$\Delta\phi_J^{\mu}$	Phase difference between a beam being reflected once at both interfaces, J and I
θ_B	Bragg diffraction angle.
$\phi_{j,B}$	Brewster angle of parallel-polarised light
$\phi_{i,t}$	Angle of total internal reflection
α	Absorption coefficient
θ_{sub}	Angle incidence in the medium of substrate
θ_0	Angle incidence in the medium of incidence
η_m	Optical admittance of the m^{th} layer
μ_0	Permeability of the free space
$\in_0$	Permittivity of the free space
χ_{ext}	Optical extraction factor
η	Optical admittance

KAJIAN TENTANG REKABENTUK DAN EKSPERIMEN KE ATAS SALUTAN MULTI LAPISAN UNTUK APPLIKASI DEDALAM PERANTI PEMANCAR CAHAYA GALLIUM NITRIDA

ABSTRAK

Dalam projek ini, cermin dan mikrorogga untuk peningkatan cahaya ultra-unggu (UV) telah dibuat dan dikaji. Kerja yang dilakukan membincang kaedah rekabentuk dua jenis cermin; jenis pertama ialah cermin pemantul Bragg teragih DBR ($Al_{0.4}Ga_{0.6}N$/ GaN) dan jenis kedua cermin dielektrik DBR (TiO_2/SiO_2, ZrO_2/SiO_2 dan HfO_2/SiO_2). Sofwer MATLAB dan analisis teori berdasarkan kaedah Pindah Matriks (TMM) digunakan untuk mengaji pantulan yang disebabkan ralat dalaman di mana ini berlaku semasa penumbuhan filem, nombor lapisan, jenis substrak dan sudut tuju. Kami anggap bahawa 10% ralat dalaman wujud pada bahan-bahan dengan indeks yang rendah dan tinggi. Keputusan simulasi kami menunjukkan ralat dalaman menyebabkan anjakan jalur pemantul sebanyak 36nm bagi struktur DBR semikonduktor dan 20nm bagi struktur DBR dielektrik. Sifat-sifat optik $Al_{0.11}Ga_{0.89}N$, $Al_{0.03}Ga_{0.97}N$, dan GaN tumbuh pada batu nilam dikajikan. Ukuran elipsometri beroperasi pada jarak gelombang 632.8nm memperolehi ψ penukaran amplitud relative bagi pengutuban p dan s, Δ anjakan fasa relatif di antara dua arah pengutuban dan indeks pemantulan, parameter-parameter yang penting untuk memajukan model bagi GaN dan substrak Al_2O_3. Kami telah menunjukkan peningkatan kecekapan ektrasi cahaya sebanyak 1.3 – 1.6 kali ganda dengan penggunaan epoksi rata dan kubah sebagai bahantara luar banding dengan udara. Keputusan simulasi menunjukkan bahawa penggunaan HfO_2 dan MgF_2 dapat meningkatkan ekstrasi cahaya dengan membelau cahaya dalaman dengan sudut pepejal yang besar ke dalam kon cahaya peleposan Tiga jenis mikrorongga telah dibuat dengan penggunaan cermin logam dan DBR dielektrik untuk peningkatan dan perencatan fotoluminescence pendarkilau (PL) dalam GaN. Struktur GaN/nilam sebagai lapisan aktif dikapitkan di antara dua cermin pemantul logam

perak. Lapisan GaN pada nilam menunjukkan puncak PL di sekitar 364 nm. Pengukuran PL menunjukkan peningkatan 2 dan 16 kali ganda pada separuh rongga cermin perak dan cermin DBR dielektrik, masing-masing. Di rongga penuh sampel, PL amplitud di tingkatkan sebanyak 10 kali bila 50 nm perak digunakan sebagai cermin hadapan. Peningkatan hebat yang melebihi 16 kali ganda diperolehi dengan penggunaan cermin perak setebal 25 nm sebagai cermin hadapan. Selain daripada itu, peningkatan hebat juga didapati dengan lubang kecil 4 mm2 dibuat di hadapan cermin dengan tebal 50 nm.

DESIGN AND EXPERIMENTAL STUDIES OF MULTILAYER COATING FOR APPLICATIONS IN GALLIUM NITRIDE LIGHT EMITTING DEVICES

ABSTRACT

In this work mirrors and microcavties for GaN-UV light enhancement were fabricated and studied. This work discusses methods of designing two types of mirror: first is the semiconductor distributed Bragg reflector (DBR) ($Al_{0.4}Ga_{0.6}N/GaN$) mirrors and second is the dielectric DBR (TiO_2/SiO_2, ZrO_2/SiO_2, and HfO_2/SiO_2) mirrors. MATLAB software and theoretical analysis based on Transfer Matrix Method (TMM) are used to investigate reflection due to depth errors that occur in films growth, number of layers, type of substrate and incidence angle. We assume that there is 10% depth error in high and low index materials. Our simulation results showed that the depth error caused the reflective band shift about 36nm for semiconductor DBR structure and 20nm for dielectric DBR structure. The optical properties of $Al_{0.11}Ga_{0.89}N$, $Al_{0.03}Ga_{0.97}N$, and GaN grown on sapphire were investigated. The ellipsometry measurement operating at wavelength 632.8nm yields ψ the relative amplitude change for p and s polarizations, Δ relative phase shift between the two polarization direction and refractive index, important parameters to develop the model for GaN on Al_2O_3 substrate. We demonstrated a GaN/sapphire microcavity exhibiting 1.3-1.6 fold enhancement in light extraction efficiency by using flat and dome epoxy as external medium compared with air as the external medium. Simulations results showed that by using HfO_2 and MgF_2 can improve the light extraction by diffracting is the internal light with a large solid angle into the escape light cone.

Three types of microcavity types were fabricated using metal and dielectric DBR mirror for the enhancement and inhibition of photoluminescence in GaN**.** A GaN/sapphire structure as an active layer was sandwiched between two mirrors, which were silver metal reflectors. GaN layer on sapphire showed a photoluminescence (PL) peak around 364 nm. Photoluminescence measurements showed intensity

enhancement of 2 and 16 fold in silver half-cavity back mirror and dielectric DBR mirror respectively. In the full cavity samples, the amplitude of the photoluminescence is enhanced 10-times when we used 50 nm silver as a front mirror. A tremendous enhancement of more than 16-fold is obtained when silver mirror of 25nm thickness was used as a front mirror. Further, a tremendous enhancement was obtained when a small hole of 4mm^2 was made in the front mirror with 50nm thickness.

CHAPTER ONE

INTRODUCTION

1.1 Introduction

Starting in early 20th century, there were several reports of light emission from materials due to applied electric fields, a phenomenon that was termed “electroluminescence”. The materials properties were poorly controlled, and the emission processes were not well understood. The first light-emitting semiconductor was a yellow-glowing piece of Silicon Carbide invented by Henry Joseph Round in 1907 (Herbert, 2002). There was not enough light to be useful, and silicon carbide is hard to work with. In 1950’s the modern light emitting diodes LEDs were based on Gallium Arsenide (GaAs) and emitted infrared light, red LEDs came next in 1960’s, using Gallium Arsenide Phosphite (GaAsP on GaAs substrate). Eventually these led to the development of high efficiency red, red-orange, and orange LEDs by changing to a GaP substrate. Mid 1970's brought Gallium Phosphite (GaP) diodes, providing greater efficiency. Mid 1980's saw the arrival of super high brightness (GaAlAsP) LEDs, first in red, then yellow. In the early 1990's, ultra bright InGaAlP LEDs were made in orange-red, orange, yellow and green. The first significant blue LEDs came in the early 1990's, using Silicon Carbide. This was a throwback to the earliest semiconductor light sources. The mid 1990's brought ultra bright blue GaN LEDs, then Indium Gallium Nitride (InGaN) LEDs, producing high-intensity green and blue. Many activities have been used on the fabrication of high brightness white/blue/green LEDs and laser diodes (LDs) in blue and UV spectra for many applications. For these purposes, III-nitride semiconductors such as gallium nitride (GaN) have been investigated for a long time. For more than 50 years ago, GaN was first synthesized by Juza and Hahn, 1938 who passed ammonia over hot gallium. This method produced small needles and platelets. Two decades later, Grimmeiss and Koelmans, 1959 studied the photoluminescence spectra of GaN. In 1969, Maruska and Tietjen succeeded in growing single crystalline GaN on sapphire using a chemical vapor deposition

technique. All the GaN films made at that time were very conductive n-type GaN (undeliberately doped). The donors were believed to be nitrogen vacancies or oxygen incorporation (Seifert *et al*., 1983). Soon after, Pankove et al., 1972, reported the first GaN LEDs. The electroluminescence spectra of these LEDs could be varied from blue to red depending on the Zn-doping concentration in the light-emitting region (Pankove, 1973). The modern progress of III nitrides began from Amano and Akasaki, (Amano *et al*., 1986). They initiated organometallic vapor phase epitaxy (OMVPE) for the growth of high quality GaN film on sapphire substrate by introducing a concept of AlN buffer layer between sapphire and GaN film. The implementation of buffer layer not only improves the crystal quality of the bulk film but also paves the way for p-type doping by using magnesium (Mg) as an acceptor doping (Amano *et al*.1988). A few years later Akasaki and Amano achieved Mg-doped p-type GaN with high conductivity using low energy electron beam irradiation (LEEBI) (Amano *et al*.1989). Then, Amano and Akasaki, 1990 demonstrated the first GaN p-n junction LED. The electroluminescence of the device was dominated by a near band edge emission at 375 nm, which was attributed to transitions involving injected electrons and Mg-associated centers in the p-GaN region. Soon thereafter, Nakamura and his colleagues at Nichia Chemicals found that thermal annealing GaN: Mg above 750°C in N_2 or vacuum also converted the material to conducting p-type (Nakamura,*et al.,* 1992). It was this breakthrough that made high brightness InGaN-based LEDs commercialize in 1994 (Nakamura, *et al.,* 1994). In 1996, the AlGaN/GaN/InGaN pulsed LD was first reported to operate at room temperature (Itaya *et al.,* 1996). An InGaN-based LD was soon successfully operated under continuous wavelength (CW) mode (Nakamura, *et al.,* 1996).

GaN and other III-nitrides are attractive in the fabrication of photonic and microelectronic devices for the most of areas because the performances of these devices are better than some of existing material systems such as Si and GaAs.

Physical, chemical and other interesting properties of GaN and related nitride materials provide the basis for the design and development of optoelectronic devices. GaN and related nitride materials can grow both in the crystalline wurtzite as well as zincblede structures, but the wurtzite structure is more common. The lattice constant of GaN wurtzite structure is shorter than that of GaN zincblede (Yoder, 1996). GaN and related nitride materials are the wide bandgap semiconductors (WBGS) whose definition is that the bandgap energy of material is larger than 3 eV. The III-nitride materials have high bond energies compared to other semiconductors therefore; normal wet etching methods is very difficult to pattern GaN and related nitrides for device fabrication (Mileham, *et al.,* 1996). Until now, photo electrochemical (PEC) etching (Minsky, *et al.,* 1999; Youtsey, *et al.,* 1997) and 10% KOH in ethylene glycol in 165 °C (Stocker, *et al.,* 1998) are the only alternative and successful wet etching techniques to process GaN. Because the sidewalls of PEC etching are very rough and high temperature of 10% KOH solution is not realistic to achieve, thus, most devices are fabricated by the techniques of plasma etching such as reactive ion etching (RIE), inductively coupled plasma (ICP) etching, and chemical assisted ion beam etching (CAIBE). Because of the GaN have direct band gap the luminous intensities of GaN-based LEDs are at least 10-100 times stronger than that of SiC LEDs and the external quantum efficiencies are almost two orders of magnitude greater than the efficiency of SiC**.** Until recently, the rapid increase in LED's efficiency was mainly due to material improvements. The saturated drift velocity is a parameter that shows the capability of device operation for high frequency at high electrical field. The electron saturated drift velocity of GaN is slightly better than that of GaAs, 8%-35% more than that of SiC, and 2.7 times higher than that of Si. The breakdown electrical field of GaN is 10 times higher than that of GaAs, 20 times larger than the breakdown field of Si. GaN presents lower dielectric constant compared to Si and GaAs. The thermal conductivity of GaN is almost 3 times higher than that of GaAs, roughly equal to that of Si, but less than one-third that of SiC. The coefficient of thermal expansion of GaN is smaller than that of GaAs and Si,

however, it exceeds 33% more than that of SiC. In wide bandgap semiconductors, GaN and SiC are always competitors on the applications of power devices. The direct bandgap and emission spectra of the photo electronic devices in the UV and visible ranges are the advantages on the applications of color displays and photodetectors (Walker, *et al.,* 1996; Monroy, *et al.,* 1999). In addition, nitride semiconductor-based LEDs have proven to be reliable in such applications as displays, lighting, indicator lights, advertisement, and traffic signs/signals There are currently major development programs in the world for three newer applications for GaN-based materials and devices (Pearton, et al., 2002), namely UV optical sources capable of operation down to 280 nm for use in airborne chemical and biological sensing systems, allowing direct multi-wavelength spectroscopic identification and monitoring of UV-induced reactions.

After giving a brief history of LED in general and GaN LED in particular, based on the properties of GaN that have been mentioned earlier in brief, GaN is deemed a key substance which has many applications, for example as a source of light operates within a wide range of spectrum depending on the mole fraction added such as (Al) and (In) to alter its energy gap. Now, modern growth techniques can achieve very high quality material deposition, giving active zones with almost 100% internal quantum efficiency, meaning that each electron-hole pair entering the active zone recombines radiatively by producing a photon. Then, the main limitation in efficiency comes from the optical extraction factor that gives the probability for an internal photon to be extracted in the outside medium. Because GaN has high refractive index it is not easy to extract light from it effectively and due to certain factors that determine light quantity emitted out of this substance. The main factors are the design and structure of this substance. The efficiency of “conventional” LEDs is limited to $(1/4n^2)$~4% where n is the refractive index of the active medium (Maxime *et al*., 2002). The remainder of internally generated light (92%–96%) never finds an opportunity to escape the emitter, and is eventually absorbed, either by the active region or the opaque substrate. For years, a significant amount of scientific work has been focused on ways of improving

the extraction efficiency of light-emitting diode (LED).). Many interesting approaches have been proposed to accomplish this, such as the use of thin light emitting layers with surface texturing (Schnitzer *et al*., 1993), resonant cavities (Temelkurana and Ozbay, 1998) and photon recycling (Misha *et al*., 1999).

This efficacy mainly depends on light reflection inside the active medium and emitting it out. Therefore the researcher tends to look for increasing the reflectivity inside the gap by using the multi-layer mirror DBR that encompasses the active medium on both ends to exploit this medium optimally. To design these DBR layers and to select its materials, there must be certain theoretical calculations through which we will be able to know the number of these layers and the ultimate reflectivity these layers provide.

The possibility of ratio error while manufacturing large number of DBR layers demand high cost of this kind of mirror which is needful to achieve high reflectivity. Through the technological development, knowing more about the materials and their properties, we can use different types of materials to achieve high reflectivity. So using the metallic reflectors in increasing the reflectivity and enhance the light emission is a cheaper and practical option. Aluminum, gold and silver are the most used metals for reflective coatings (Macleod, 1986).

The objectives of the thesis are as follows:

1- Simulation of DBR for semiconductors (GaN /$Al_xGa_{1-x}N$) and dielectric (TiO_2/SiO_2, ZrO_2/SiO_2, HfO_2/SiO_2) materials to achieve high reflectivity.
2- Simulation of GaN microcavity using external materials (HfO_2, MgF_2, and epoxy).

3- Characterization of GaN material as active mediums using different optical techniques (ellipsometry, filmetrics, spectrophotometer, and photoluminescence).
4- Fabrication and measurement of metal/sapphire and dielectric/sapphire DBR mirrors.
5- Design and fabrication of half and full microcavities on GaN using metal and dielectric DBR mirrors to get high extraction efficiency.
6- Fabrication of external medium using epoxy in order to get high extraction efficiency from the active medium.

The originality of our work is firstly, using the silver as a contact and as a resonator instead of multilayer semiconductor or dielectric materials to enhance the extraction efficiency from GaN active layer. Secondly, in our microcavity design we have used the sapphire substrate as a spacer between the back mirror and the active medium to get resonance condition to achieve standing wave inside the active medium and enhance the extracted light.

This thesis is organized as follows: In chapter 2, TMM theory of the DBR optical multilayer and calculation on reflectivity and transmissivity will be presented. Chapter 3 describes the results from MATLAB programs to simulate and analize the effects of variation of certain parameters on DBR efficiency. This will provide sufficient background to enable one to understand the microcavity operation and the effects of these parameters on UV light emission enhancement. Chapter 4 discusses the fabrication and measurement results of the active medium and the dielectric DBR and metal (Ag, Al) mirrors. Chapter 5 focuses on results of PL intensity enhancement using metal (Ag, Al) and dielectric DBR mirrors in microcavity to enhance the spontaneous UV emission in GaN samples. Finally, Chapter 6 concludes the thesis, with summary and future work.

CHAPTER TWO

MULTILAYER STRUCTURE AND MICROCAVITY DESIGN

2.1 Introduction

This chapter discusses the optical properties of thin films and how their unique characteristics can be used to develop the reflectivity, and enhance the extracted light using microcavity. One of the most important and pervasive sub-fields of optical science is the technology of thin film. It is very rare to find any optical system in today's technology that does not have components with single or multilayer thin films attached.

The physical phenomena that describe the basis of filters (mirrors) include absorption, refraction, diffraction, scattering and polarization. The optical performances of thin film filters are determined by the interference that occurs because of multiple reflected beams at the various interfaces within the film coating (Flory, 1995; Conway, 1999). However the most complete descriptions of the performance of these filters are provided by the spectral reflectance, transmittance, absorption and phase shift on reflection (Macleod, 2000; Furman *et al*., 1992). This section briefly details the basic theory, which is necessary in order to make calculations of the properties of multilayer thin film filters.

2.2 Optical parameters of thin films

The theoretical and experimental studies on the optical behaviors of thin films deal primarily with optical reflection, transmission, and absorption properties, and their relation to the thickness and optical constants of films. Consequently, complex multilayer optical-device systems with remarkable reflection, antireflection, interference, and polarization properties have emerged for both laboratory and industrial applications. The simplest and commonest type of optical coating is probably the thin metal layer that is used as a reflector. Metals attenuate very rapidly any light that succeeds in passing through their front surface. Thus a thin metal film will usually have optical properties indistinguishable from those of the bulk material. Almost other thin

film optical coatings depend on interference for their operation. In an optical coating, the particular materials used for the thin film vary with the application and consideration, such as the environment in which the coating will be used, frequently imply that the choice of materials should be as much for their mechanical as for their optical properties. It is possible to construct assemblies of thin films which will reduce the reflectance of surface and hence increase the transmittance of a component, or increase the reflectance of a surface, or which will give high reflectance and low transmittance over part of a region and low reflectance and high transmittance over the remainder, or which will have different properties for different planes of polarization and so on (Thelen, 1988). Thin film coating are often known by names which describe their function, such as antireflection coatings, beam splitters, polarizer, long wave pass filters, band-stop or minus filters, or which describe their construction, such as quarter-wave attack or quarter-half quarter coating (Furman and Tikhonravov, 1992).

2.2.1 Refractive index

The indices of refraction are only properties of an optical material, which used in actual design of optical system. A refracting material, to be useful, obviously must transmit radiation in the wavelength region in which it is to be used. In some instances, the refracting material transmits imperfectly in the region of use and the designer must determine what thickness he can use without greatly impairing the performance of the instrument. In most cases, the thickness and refractive index of the films in a multilayer mirror are chosen from theoretical considerations. In order to translate this design into a practical mirror, it is necessary to select for each layer a thin film material, which can be evaporated to a desired thickness and which has a refractive index, which is close to the theoretical value.

2.2.2 Quarter wave optical thickness and optical admittance

The principle of the single and multilayer reflection coatings is based on the constructive interference of light reflected from the interfaces of the coating layers. Any time light traverses an interface between two media with different refractive indexes, such as the air/sapphire interface, a portion of the incident light is reflected. When this incident light is normal to the surface, the amplitude of the reflected wave at the interface between the sapphire substrate and the incident media is proportional to the Fresnel amplitude reflection coefficient (r) (Born and Wolf, 1983):

$$r = \frac{(n_0 - n_s)}{(n_0 + n_s)} \qquad (2\text{-}1)$$

where n_0 is the refractive index of the incident medium (usually air), and n_s is the refractive index of the substrate, in this case sapphire. The human eye and most other photodetectors, however, do not respond directly to the amplitude of light, but rather to the intensity of light. The intensity of the reflected light, referred to as reflectivity (R), is equal to the square of the amplitude of the reflected light. The reflectivity of a bare substrate, irradiated at normal incidence is given by,

$$R = r^2 = 1 - T = \frac{(n_0 - n_s)^2}{(n_0 + n_s)^2} \qquad (2\text{-}2)$$

where T is the transmittance. For example, the amplitude of the light reflected off uncoated sapphire ($n_s = 1.78$) in air ($n_0 = 1$) is $|r| = 0.28$. The reflectivity in this situation is $R = r^2 = 0.078$, or 7.8%. Therefore, as far as the human eye and other photodetectors are concerned, 7.8% of the light is reflected off the sapphire substrate. When this sapphire substrate is coated with a thin layer (non-absorbing) film of different index than the sapphire, the reflectivity is changed. The reflectivity of a surface coated with a single layer having refractive index n_1 and physical thickness t_1 is given (Macleod., 1986):

$$R = 1 - T = \frac{(n_0 - n_s)^2 \cos^2 \delta_1 + \left(n_1 - n_0 \frac{n_s}{n_1} \right)^2 \sin^2 \delta_1}{(n_0 + n_s)^2 \cos^2 \delta_1 + \left(n_1 + n_0 \frac{n_s}{n_1} \right)^2 \sin^2 \delta_1} \quad \text{(2-3)}$$

$$\delta_1 = 2\pi \frac{n_1 t_1}{\lambda_0} \quad \text{(2-4)}$$

where δ_1 is the phase retardation in the thin film layer, and λ_0 is the wavelength of incident light in a vacuum. The product $n_1 t_1$ is referred to as the optical thickness of the film.

This product is what determines the phase shift of a light beam as it traverses the film. When the optical thickness of the layer is equal to ($m\lambda_0/2$), where m is an odd integer, the phase shift suffered by a wave traveling through thickness t_1 of a thin film is given by ($-\pi n_1 t_1 / \lambda_0$), the phase shift multiple of 180º and the layer acts as an absentee layer. In this case equation (2-3) reduces to equation (2-2) and the reflectivity of the coated substrate is the same as that of the uncoated substrate. The optical thickness $n_1 t_1$ is related to physical thickness by the refractive index. If the optical thickness is ($\lambda_0/4$) then, $t_1 = \lambda_0 / 4n_1$ and the layer is referred to as having quarter wave optical thickness (QWOT). Fig. 2.1 shows a comparison between the optical and physical thickness of a film. The optical thickness is shown to be greater than its physical thickness. This difference is compensated for by the fact that the wavelength shown is not the wavelength in the film, but the wavelength in a vacuum.

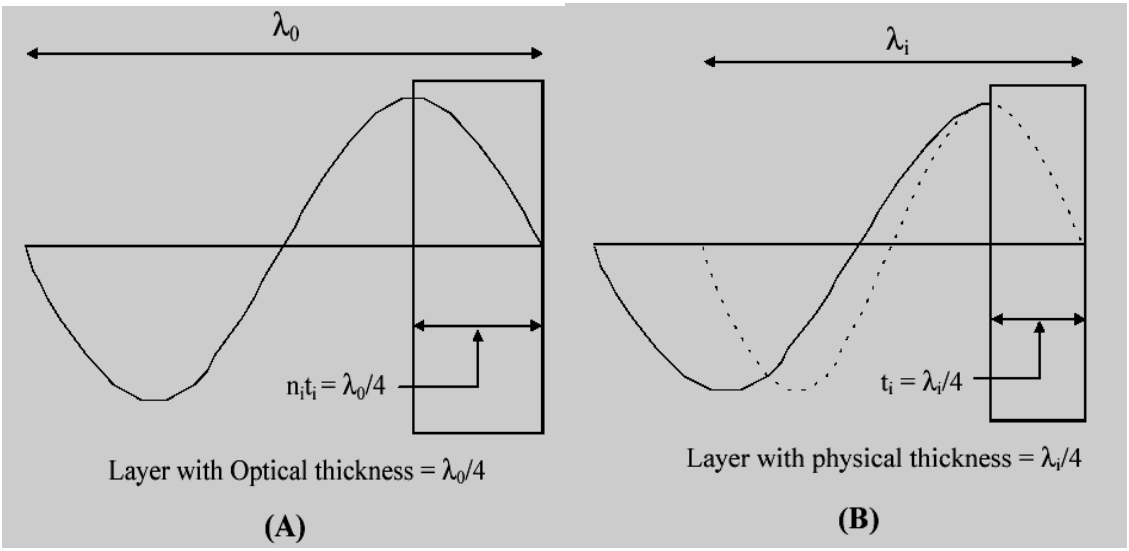

Fig. 2.1: Comparison between physical and optical thickness in an optical film.

The optical thickness of the film is represented in (A) and the physical thickness is shown in (B). The solid lines represent the wavelength of light in a vacuum, and the dotted line represents the wavelength in the film. The wavelength of the incident light after it has entered the film is represented by the dotted line. This illustrates that the wavelength of the light decreases as it enters the film.

The wavelength (λ_i) of the incident light as it propagates through the thin film layer is $\lambda_i = \lambda_0 / n_1$. It is usual to define some extra quantities to reduce the notation of the reflectance and transmittance expressions. Instead of the refractive index, it is common to use the quantity $\eta = n/(c\mu)$ (ratio of magnetic field to electric field strengths) known as the characteristic optical admittance of the medium. In free space, the optical admittance is (Liddell, 1980):

$$\eta_0 = (\frac{\in_0}{\mu_0})^{\frac{1}{2}} = 2.6544 \times 10^{-3}\ \text{S} \qquad (2\text{-}5)$$

$\in_0$ and μ_0 are the permittivity and the permeability of the free space respectively.

And since $\in_0 = 1/(\mu_0 c^2)$ and at optical frequencies $\mu = \mu_0$, we can write:

$$\eta = n\eta_0 \qquad (2\text{-}6)$$

The straightforward nature of the calculations when the layer is a quarter-wave thick yields a particularly simple result that can be best expressed in terms of the transformation of the admittance of the substrate. Optical quarter wave layer of characteristic admittance η transform the admittance of the substrate surface from η_s to η^2/η_s. This result is known as the quarter-wave rule and the reflectance of the substrate coated with a single quarter-wave layer is then:

$$R = \left(\frac{\eta_0 - \eta^2/\eta_s}{\eta_0 + \eta^2/\eta_s} \right)^2 \qquad (2\text{-}7)$$

We can extend the idea of admittance transformation by optical quarter wave layer to a stack of quarter waves.

The summary of the discussion of this section can be seen in Fig. 2.2, which shows that the effects of the refractive index and thin film optical thickness on reflectivity by using different thin film materials on the same substrate, (sapphire). Also shown in Fig. 2.2 the reflectance of uncoated sapphire can be calculated as 7.8% because of the index contrast between the air and sapphire and so this simple coating of quarter-wave of silicon dioxide (SiO_2) acts to reduce the reflectance by a very significant amount. In fact this coating is a very simple example of an antireflection coating. Clearly, a high admittance quarter-wave layer will increase the reflectance of a sapphire surface such as TiO_2, GaN, and HfO_2.

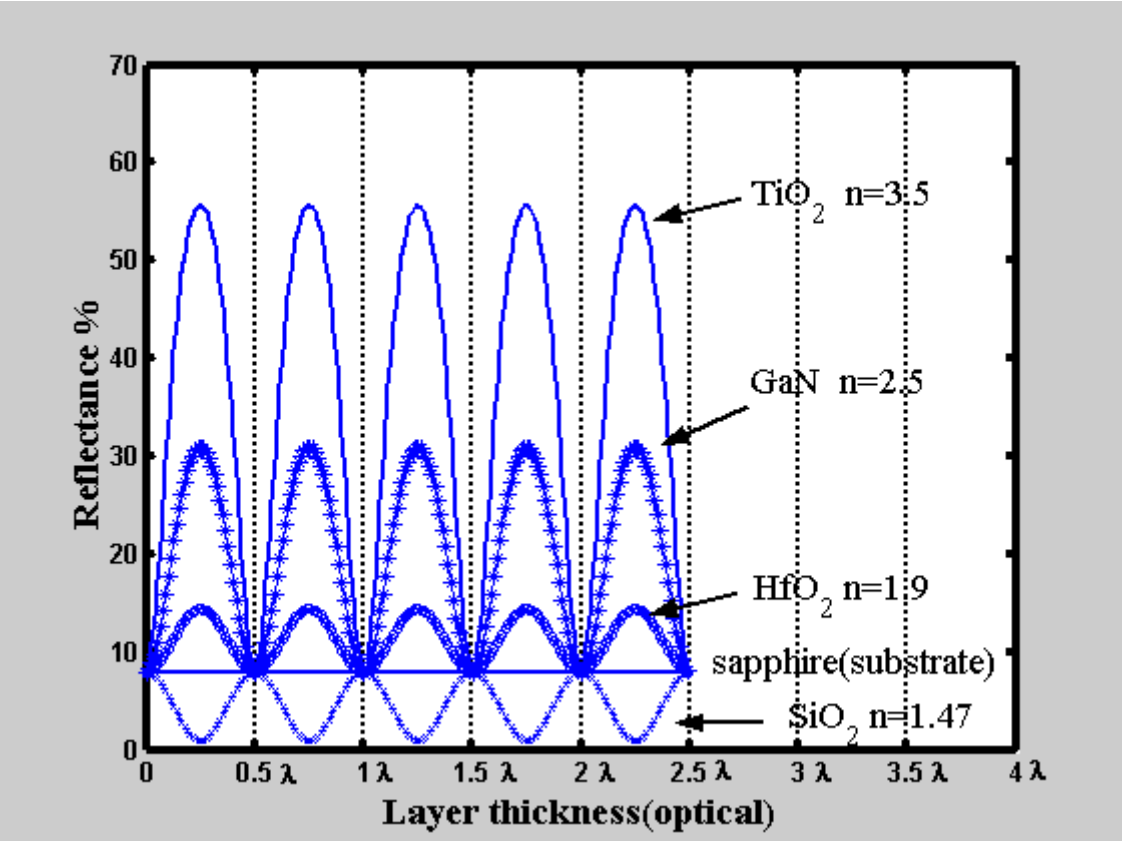

Fig. 2.2: The reflectance of single films of different index on sapphire as a function of optical thickness.

2.3 Transfer matrix method (TMM)

2.3.1 Single and double layers reflectivity

Optical filters can be defined as thickness dependent refractive index systems, which modify the properties of a surface to produce the desired optical characteristics. As discussed previously, thin film interference filters are highly popular for applications in a range of fields. These filters can work over a broad range of wavelengths or over a narrow band. A simple extension of the analysis in section (2.2.2) as shown in Fig. 2.2 can be used to analyze the reflectance of a thin film.

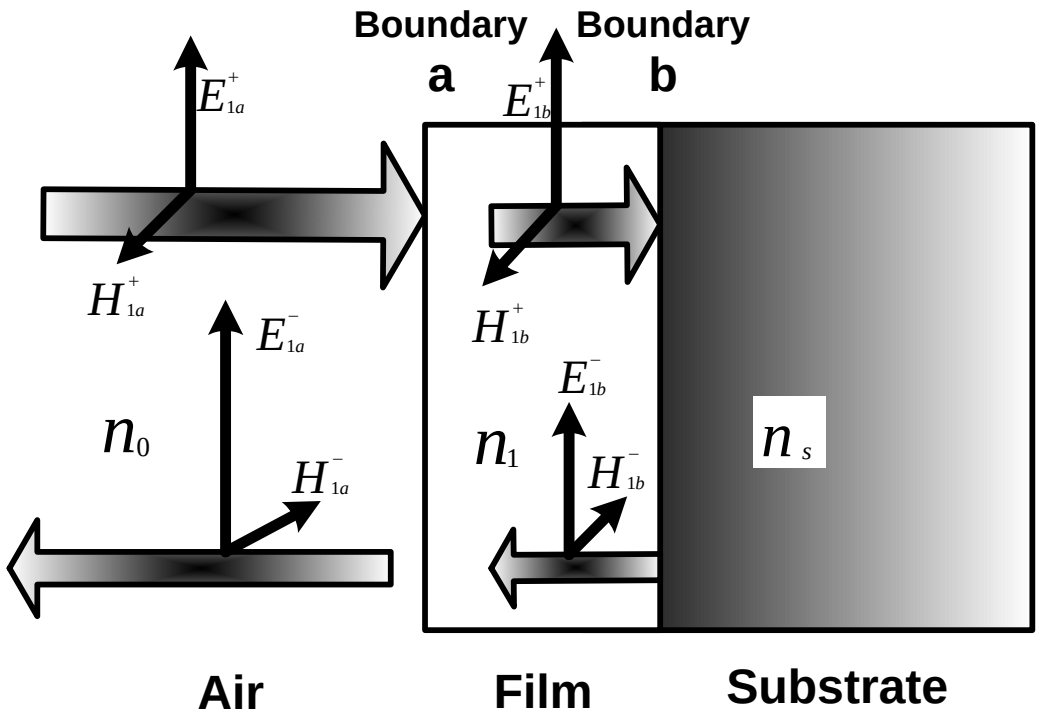

Fig. 2.3: Plane wave incident on a thin film

The successive reflections at the multiple interfaces give rise to multiple beams and the summation of these beams determines the properties of the film. The film is said to be 'thin' when interference effects can be observed in the beams. When monochromatic, plane polarized light passes through a thin film, multiple reflections at the interfaces give rise, generally, to two main beams of light advancing in opposite directions. At any point within the medium, these beams will interfere and give rise to a resultant electric field E and a resultant magnetic field H. Considering the light to be incident normally to the surface; the field vectors are parallel to the interfaces.

The arrangement is illustrated in Fig. 2.3. At this stage it is convenient to introduce a new notation. We denote waves in the direction of incidence by the symbol + (that is, positive-going) and waves in the opposite direction by – (that is, negative-going). The interface between the films and the substrate, denoted by the symbol "b",

can be treated in exactly the same way as the simple boundary in a and b. We consider the tangential components of the fields. There is no negative-going wave in the substrate and the waves in the film can be summed into one resultant positive-going wave and one resultant negative-going wave. At this interface, then, the tangential components of E and H are

$$E_b = E_{1b}^{+} + E_{1b}^{-} \tag{2-8}$$

$$H_b = \eta_1 H_{1b}^{+} - \eta_1 H_{1b}^{-} \tag{2-9}$$

where η_1 is the optical admittance of the thin film layer which is defined by the optical admittance of the free space ($\eta_0 = 1/377$ siemens) as:

$$\eta_1 = n_1 \eta_0 \tag{2-10}$$

At normal incident angle, the optical admittance is usually normalized to equal the same numerical magnitude as the refractive index. At oblique incidence angles, the wave is split in two plane polarized components. One with the electric vector in the plane of incidence, known as p-polarized (TM, transverse magnetic field) and one with electric vector normal to the plane of incidence, known as s-polarized (TE, transverse electric field), as shown in Fig. 2.4.

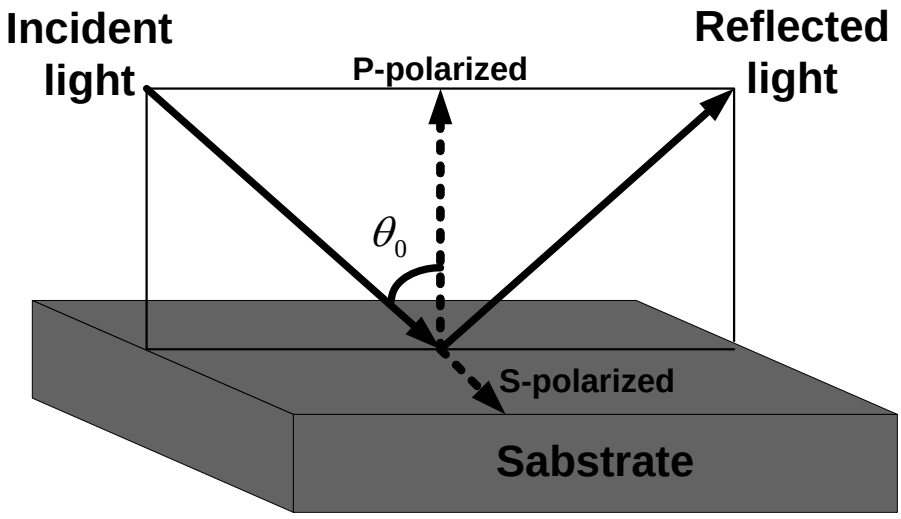

Fig. 2.4: The light at oblique incidence angles, the wave is split two plane polarized components.

The optical admittance at oblique incidence angle can be expressed as:

$\eta_1 = n_1 \eta_0 \cos\theta_1$ for s-polarization (2-11)

$\eta_1 = (n_1 \eta_0)/\cos\theta_1$ for p-polarization (2-12)

where θ_1 is the angle of incidence in the thin film layer, which is related to the angles of incidence in the medium of incidence θ_0 and in the substrate θ_{sub} by Snell's laws (Heavens, 1955):

$$n_0 \sin\theta_0 = n_1 \sin\theta_1 \quad (2\text{-}13)$$

$$n_1 \sin\theta_1 = n_{sub} \sin\theta_{sub} \quad (2\text{-}14)$$

From equations (2-8) and (2-9), where we are neglecting the common phase factors we can obtain the expression for the traveling waves (Ulaby, 1999):

$$E_{1b}^{+} = \frac{1}{2}\left(\frac{H_b}{\eta_1} + E_b\right) \quad (2\text{-}15)$$

$$E_{1b}^{-} = \frac{1}{2}\left(-\frac{H_b}{\eta_1} + E_b\right) \quad (2\text{-}16)$$

Hence:

$$H_{1b}^{+} = \eta_1 E_{1b}^{+} = \frac{1}{2}\left(H_b + \eta_1 E_b\right) \quad (2\text{-}17)$$

$$H_{1b}^{-} = -\eta_1 E_{1b}^{-} = \frac{1}{2}\left(H_b - \eta_1 E_b\right) \quad (2\text{-}18)$$

these are the amplitude terms for the fields at the interface "b". A wave traveling inside the material exponential fall-off amplitude, therefore the expression of the fields at interfaces "a" are the same as at "b" but affected by the appropriate phase factors. The phase factor of the positive-going wave will be multiplied by $\exp(i\delta)$ where $\delta = 2\pi n_1 d \cos\theta_1/\lambda$ while the negative-going phase factor will be multiplied by $\exp(-i\delta)$. The values of E and H at the interface are now, using equations (2-15) to (2-18),

$$E_{1a}^{+} = E_{1b}^{+}\, e^{i\delta} = \frac{1}{2}\left(\frac{H_b}{\eta_1} + E_b\right) e^{i\delta} \tag{2-19}$$

$$E_{1a}^{-} = E_{1b}^{-}\, e^{-i\delta} = \frac{1}{2}\left(-\frac{H_b}{\eta_1} + E_b\right) e^{-i\delta} \tag{2-20}$$

$$H_{1a}^{+} = H_{1b}^{+}\, e^{i\delta} = \eta_1 E_{1b}^{+} = \frac{1}{2}\left(H_b + \eta_1 E_b\right) e^{i\delta} \tag{2-21}$$

$$H_{1a}^{-} = H_{1b}^{-}\, e^{-i\delta} = -\eta_1 E_{1b}^{-} = \frac{1}{2}\left(H_b - \eta_1 E_b\right) e^{-i\delta} \tag{2-22}$$

The resultant field in “a” are:

$$E_a = E_{1a}^{+} + E_{1a}^{-} = E_b\left(\frac{e^{i\delta} + e^{-i\delta}}{2}\right) + H_b\left(\frac{e^{i\delta} - e^{-i\delta}}{2\eta_1}\right)$$

$$= E_b \cos\delta + H_b \frac{i\sin\delta}{\eta_1} \tag{2-23}$$

$$H_a = H_{1a}^{+} + H_{1a}^{-} = E_b\eta_1\left(\frac{e^{i\delta} - e^{-i\delta}}{2}\right) + H_b\left(\frac{e^{i\delta} + e^{-i\delta}}{2\eta_1}\right)$$

$$= E_b\, i\eta_1 \sin\delta + H_b \cos\delta \tag{2-24}$$

This can be written in matrix notation, defining the whole thin film between the ‘boundary a’ and ‘boundary b’ as shown in Fig. 2.3 which is given by:

$$\begin{bmatrix} \cos\delta & \dfrac{i\sin\delta}{\eta_1} \\ i\,\eta_1 \sin\delta & \cos\delta \end{bmatrix} \tag{2-25}$$

Therefore, we can write the matrix for single layer as,

$$\begin{bmatrix} E_a \\ H_a \end{bmatrix} = \begin{bmatrix} \cos\delta & \dfrac{i\sin\delta}{\eta_1} \\ i\,\eta_1 \sin\delta & \cos\delta \end{bmatrix} \begin{bmatrix} E_b \\ H_b \end{bmatrix} \tag{2-26}$$

Since the tangential components of E and H are continuous across a boundary, and since there is only a positive-going wave in the substrate, this relationship connects the tangential components of E and H at the incident interface with the tangential components of E and H, which are transmitted through the final interface. The 2x2 matrix on the right-hand side of equation (2-26) is known as the characteristic matrix of the thin film.

We define the input optical admittance Y of the assembly as

$$Y = \frac{H_a}{E_a} \tag{2-27}$$

when the problem becomes merely that of finding the reflectance R of a simple interface between an incident medium of admittance η_0 and a medium of admittance Y, i.e.

$$r = \frac{\eta_0 - Y}{\eta_0 + Y} \tag{2-28}$$

$$R = \left(\frac{\eta_0 - Y}{\eta_0 + Y}\right)\left(\frac{\eta_0 - Y}{\eta_0 + Y}\right)^* \tag{2-29}$$

We can normalize equation (2-26) by dividing by E_b to give

$$E_a = \begin{bmatrix} 1 \\ Y \end{bmatrix} = \begin{bmatrix} B \\ C \end{bmatrix} = \begin{bmatrix} \cos\delta & (i\sin\delta)/\eta_1 \\ i\eta_1 \sin\delta & \cos\delta \end{bmatrix} \begin{bmatrix} 1 \\ \eta_{sub} \end{bmatrix} E_b \tag{2-30}$$

B and C, the normalized electric and magnetic fields at the front interface, are the quantities from which we will be extracting the properties of the thin-film system. Clearly, from (2-27) and (2-30), we can write

$$Y = \frac{\eta_{sub}\cos\delta + i\eta_1 \sin\delta}{\cos\delta + i(\eta_{sub}/\eta_1)\sin\delta} \tag{2-31}$$

and from (2-29) and (2-31) we can calculate the reflectance.

Let another film be added to the single film of the previous figure so that the final interface is now denoted by c, as shown in Fig. 2.5.

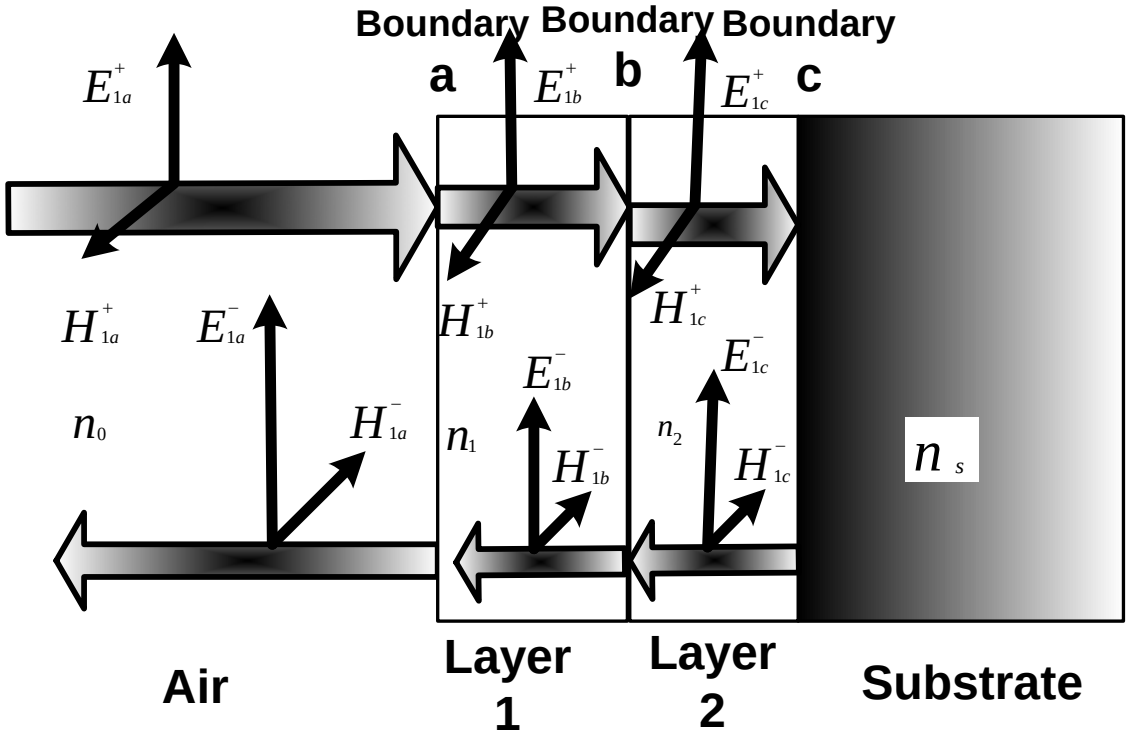

Fig. 2.5: Schematic diagram showing the interfaces of double layer structure.

The characteristic matrix of the film nearest the substrate is

$$\begin{bmatrix} \cos\delta_2 & (i\sin\delta_2)/\eta_2 \\ i\eta_2\sin\delta_2 & \cos\delta_2 \end{bmatrix} \tag{2-32}$$

$$\begin{bmatrix} E_b \\ H_b \end{bmatrix} = \begin{bmatrix} \cos\delta_2 & (i\sin\delta_2)/\eta_2 \\ i\eta_2\sin\delta_2 & \cos\delta_2 \end{bmatrix} \begin{bmatrix} E_c \\ H_c \end{bmatrix} \tag{2-33}$$

and the characteristic matrix of the double film assembly becomes

$$\begin{bmatrix} E_a \\ H_a \end{bmatrix} = \begin{bmatrix} \cos\delta_1 & (i\sin\delta_1)/\eta_1 \\ i\eta_1\sin\delta_1 & \cos\delta_1 \end{bmatrix} \begin{bmatrix} \cos\delta_2 & (i\sin\delta_2)/\eta_2 \\ i\eta_2\sin\delta_2 & \cos\delta_2 \end{bmatrix} \begin{bmatrix} E_c \\ H_c \end{bmatrix} \tag{2-34}$$

$$\begin{bmatrix} B \\ C \end{bmatrix} = \begin{bmatrix} \cos\delta_1 & (i\sin\delta_1)/\eta_1 \\ i\eta_1\sin\delta_1 & \cos\delta_1 \end{bmatrix} \begin{bmatrix} \cos\delta_2 & (i\sin\delta_2)/\eta_2 \\ i\eta_2\sin\delta_2 & \cos\delta_2 \end{bmatrix} \begin{bmatrix} 1 \\ \eta_{sub} \end{bmatrix} \tag{2-35}$$

Y, is as before equal to C/B, and the amplitude reflection coefficient and the reflectance are the same equations above. The result can be immediately extended to the general case of an assembly of N layers.

2.3.2 Multilayer calculation

2.3.2.1 Distributed Bragg Reflector (DBR) mirror

The distributed Bragg reflector (DBR) with high reflectance should help to develop devices such as lasers and light emitting diodes. DBR mirror can simply be described as a stack of thin film structure of alternating high and low refractive index films, all one quarter wavelength thick (Fig. 2.6). By employing all layers with quarter wavelength thickness with alternating high and low refractive indices, upon incidence the light beams reflected at successive boundaries throughout the assembly are equal in phase when they reappear at the front surface. These will recombine constructively producing high reflectivity with phase change upon reflection of 180^o or 0^o (Macleod, 2000). This effect leads to the formation of a so-called stop band in the vicinity of the Bragg wavelength.

For ideal mirror without any absorption, the reflectivity can reach any desired value between 0% and almost 100% by adding layer pairs and thereby decreasing the mirror transmission. A highly reflective DBR allows the fabrication of efficient vertical cavity surface emitting lasers (VCSEL) (Roux *et al*., 1999) and bright light emitting diodes (LED) (Uusimaa *et al*., 1998). Successful examples include both II-VI and III-V compound semiconductor-based VCSELs and bright LEDs (Beak *et al*., 1999, Naranjo e*t al*., 2002). DBR mirrors are more commonly studied in LEDs than metallic mirrors since its advantages over metallic mirrors are, it is wavelength selective and it also provide better enhancement factor upon light emission. Its reflectivity can easily be

controlled and increasing reflectivity doesn't result in absorption losses compared to metallic mirrors.

This section will look into the DBR design and investigate its reflectivity and transmission properties. The parameters that determined and performance high reflectivity are thickness, number of layers and optical parameters.

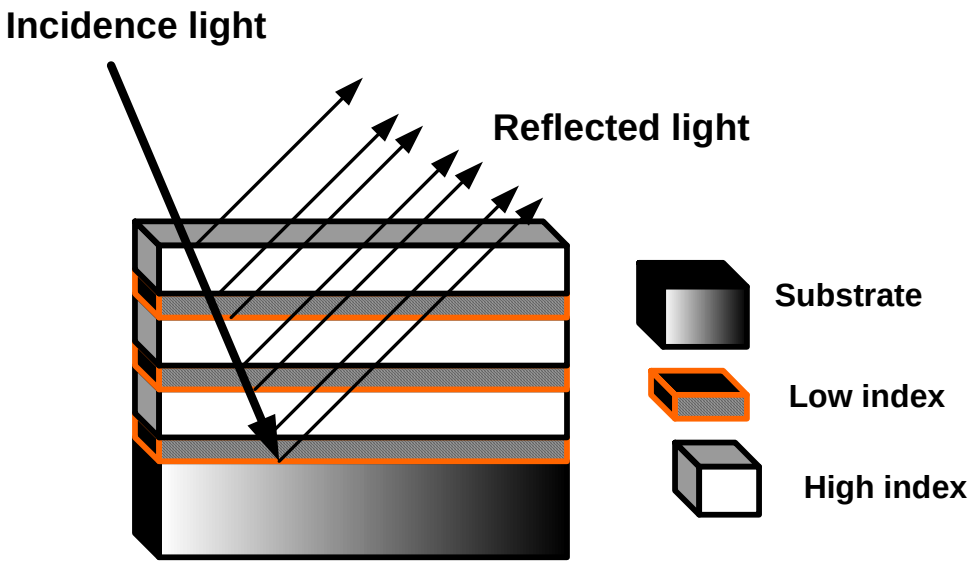

Fig. 2.6: DBR mirror structure

Various methods have been developed to calculate the multilayer reflectivity and the most convenient method is the matrix method. The matrix method for calculating the spectral coefficients of the layered media was first suggested by (Berreman, 1986) and has been widely employed ever since.

Let us assume a multilayer coating consisting of a finite number of homogeneous and isotropic layers (see Fig. 2.7).

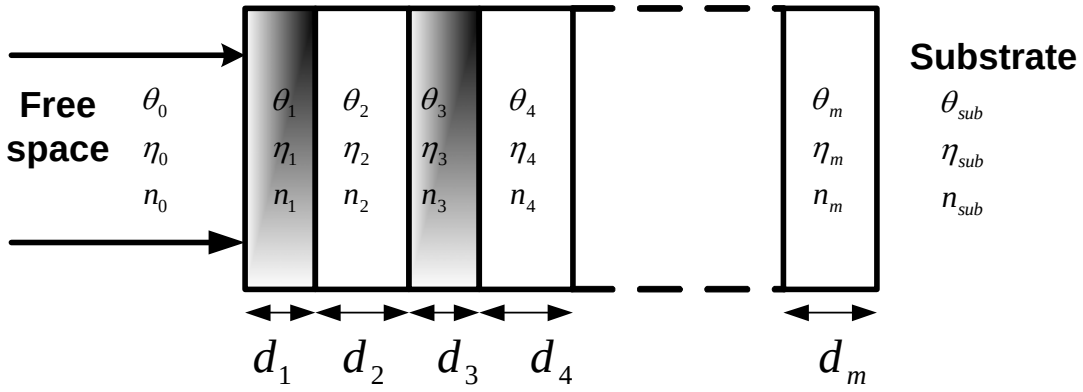

Fig. 2.7: Multilayer coating including m[th] homogeneous layers

In Fig. 2.6, the geometrical thickness of the layers are denoted as $d_1, d_2, ...d_m$, and their refractive indices as $n_1, n_2, ...n_m$, where m denotes the total number of layers. Next, the incident angle will be denoted as θ_0 and its refractive index as n_0. Refractive index of the substrate, it will be denoted as n_{sub}. By applying the boundary condition for the propagation of an electromagnetic (EM) wave at the interface between the $(m-1)$ and the m^{th} layer, the matrix expression is:

$$\begin{bmatrix} E_{m-1} \\ H_{m-1} \end{bmatrix} = \begin{bmatrix} \cos\delta_m & (i\sin\delta_m)/\eta_m \\ i\eta_m \sin\delta_m & \cos\delta_m \end{bmatrix} \begin{bmatrix} E_m \\ H_m \end{bmatrix} \quad (2\text{-}36)$$

$$\eta_m = n_m \eta_0 \quad (2\text{-}37)$$

For N-layers the expression is

$$\begin{bmatrix} E_0 \\ H_0 \end{bmatrix} = \prod_{m=1}^{N} M_m \begin{bmatrix} E_N \\ H_N \end{bmatrix} \quad (2\text{-}38)$$

where

$$M_m = \begin{bmatrix} \cos\delta_m & (i\sin\delta_m)/\eta_m \\ i\eta_m \sin\delta_m & \cos\delta_m \end{bmatrix} \quad (2\text{-}39)$$

and

$$\begin{bmatrix} E_N \\ H_N \end{bmatrix} = \begin{bmatrix} 1 \\ \eta_s \end{bmatrix} E_s \qquad (2\text{-}40)$$

where δ_m is the phase shift of the EM wave at the interface obtained from equation (2-4). From equation 2-37 we can obtained η_m and η_s which is the optical admittance of the m^{th} layer and the substrate respectively. Equation 2-40 can be expressed as:

$$E_N \begin{bmatrix} 1 \\ Y \end{bmatrix} = \begin{bmatrix} 1 \\ \eta_s \end{bmatrix} E_s \qquad (2\text{-}41)$$

Where Y is the characteristic optical admittance defined by equation 2-37. For a general case of assembly of N layers, the characteristic matrix is simply the product of the individual matrices taken in the correct order and is denoted by:

$$\begin{bmatrix} B \\ C \end{bmatrix} = \left\{ \prod_{m=1}^{N} \begin{bmatrix} \cos\delta_m & (i\sin\delta_m)/\eta_m \\ i\eta_m \sin\delta_m & \cos\delta_m \end{bmatrix} \right\} \begin{bmatrix} 1 \\ \eta_s \end{bmatrix} \qquad (2\text{-}42)$$

B and C are the total electric and magnetic field amplitudes; their ratio has the dimension of admittance.

$$Y = C/B \qquad (2\text{-}43)$$

Y is the admittance presented to the incident wave by the coating. The admittance presented by simple interface between two media is indistinguishable from the reflectance at that interface. This concept is used to calculate the reflectance of an assembly of thin films and the transmittance and be derived through the relationship of $T = (1-R)$. The expressions for reflectance, transmittance and phase changes on reflection are given respectively as follows:

$$R = \left[\frac{\eta_0 B - C}{\eta_0 B + C}\right]\left[\frac{\eta_0 B - C}{\eta_0 B + C}\right]^* \quad (2\text{-}44)$$

$$T = \frac{4\eta_0 \ \mathrm{Re}\,\eta_{sub}}{(\eta_0 B + C)(\eta_0 B + C)^*} \quad (2\text{-}45)$$

Where "$*$ "denote the conjugate and the phase changes on reflection are then given by:

$$\Psi = \arg\left[\frac{\eta_0 B - C}{\eta_0 B + C}\right] \quad (2\text{-}46)$$

2.3.2.2 MATLAB simulation programs

Part of this thesis is to model and investigate the DBR mirror properties of microcavity enhancement. It was decided that simulation via a software program would be the best option. Previous section showed that the theory and formulas could be used to accurately determine the reflectivity performance of an assembly of layers.

The design of thin-film multilayer coating often specifies the transmittance and reflectance values at a number of wavelengths, angles, and polarizations of the incident light. Hence, the MATLAB programs are written as a function of the parameters that can be used to reach these goals, such as the number of layers in the multilayer, the layer thicknesses, and the refractive indices of the individual layers and surrounding media. The following sections outline the basic structure of MATLAB programs a step by step approach will be adopted using equation shown in the previous section. The MATLAB source codes for calculating reflectivity of the DBR mirrors are enclosed in Appendix A. MATLAB source codes for phase shift of DBR mirrors are enclosed in Appendix B. The progressive steps, taken to obtain the program are outlined in the flowchart of Fig. 2.8.